Journal of Applied Polymer Science

Defining a strain-induced time constant for oriented low shear-induced structuring in high consistency MFC/NFC-filler composite suspensions

Katarina Dimic-Misic,[1] Thaddeus C. Maloney,[1] Patrick A. C. Gane[1,2]

[1]Department of Forest Products Technology, School of Chemical Technology, Aalto University, 00076 Aalto, Helsinki, Finland

[2]Omya International AG, Baslerstrasse 42, CH-4665 Oftringen, Switzerland

Correspondence to: K. Dimic-Misic (E-mail: katarina.dimic.misic@aalto.fi)

ABSTRACT: Micro and nanofibrillated cellulose is an essentially one-dimensional high aspect-ratio particle material, which can undergo two-dimensional layer (band) structuring under shear. Controlling the evolving rheological properties in aqueous suspension is essential for industrial applications in composite materials. This study focuses on an as yet considered to be unreported phenomenon of structure hardening under low shear. The timescale of the quasi gelation-controlled structure formation under low shear is studied using the large gap vane-in-cup geometry of the Brookfield viscometer. It is proposed that localized structure forms within continuous shear bands, similar to quasi liquid-crystal formation. By extrapolating a characteristic structure growth parameter to the rotation speed at which it becomes zero, the strain-induced structure time constant, t_{gel}, can be obtained as $\dot{\gamma}(= f(\Omega)) = 1/t_{gel}$ for the range $\Omega = 10$–100/min. The time constant of low shear structure formation is shown to be separable from the static viscoelastic structure build under oscillation in concentrated composite suspension using plate-plate geometry, which is manifest by a Weissenberg normal force response on switching to applied shear, when the time constant of structuration t_{gel} is long. © 2015 Wiley Periodicals, Inc. J. Appl. Polym. Sci. **2015**, *132*, 42827.

KEYWORDS: biopolymers & renewable polymers; composites; nanostructured polymers; rheology; structure-property relations

Received 2 June 2015; accepted 9 August 2015

DOI: 10.1002/app.42827

INTRODUCTION

Sustainability is one of the key targets for industrial practice today, and research aimed at new composite materials based on renewable sources is considered highly relevant. In the forest products industry, nano-scale cellulose fibrils (NFC), microfibrillated (MFC), and nanofibrillated microfibres (MNFC) have attracted the attention as potential materials for emerging bio-based applications. There are several methods to produce nano-scale fibrils. Chemical methods are frequently employed either alone or in combination with mechanical fibrillation. One such is the production of NFC applying aqueous TEMPO-mediated oxidation, in which the primary hydroxyl groups of cellulose are oxidized into carboxylate groups, resulting in strong electrostatic repulsion between the fibrils which in turn prevents formation of strong inter-fibrillar hydrogen bonding during centration.[1]

Mechanical methods include high pressure homogenizers, micro-fluidic cells, rotor-stators, refiners, or micro-grinders to break up the wood fibres to dimensions of 20–50 nm in diameter.[2–4]High consistency composite materials consisting of a mixture of traditional pulp fibres and NFC and MFC), as well as intermediary microfibrillar materials with nanofibrillation applied on their surface (collectively termed here as MNFC) are attracting much attention.[5] Such composites are additionally attractive due to the possibility to include high levels of mineral fillers by taking advantage of the increased strength imparting properties of MNFC through increased numbers of hydrogen bonding contact points in the fibre-filler matrix.[6,7] Highly charged MNFC hydrophilic material behaves similarly to a superabsorber polymer, in that the attraction to water results in a high osmotic pressure leading to bound and interstitial water molecules clustered within a swollen gel even at very low mass concentrations.[8–10] The rheological characteristics of these materials generally show shear thinning and, due to network formation, yield stress with typical non-linear flow curves, which display thixotropy.[11,12] Avoiding wall-slip in such material suspensions frequently requires use of serrated plate-plate geometry or vane-in-cup geometry.[10–13]

Although wall-slip may be eliminated with use of the vane-in-cup, there is no guarantee that application of such geometry will eliminate shear banding acting as a precursor to internal boundaries forming between regions of aligned planar structure.[11,12] The importance of using a correction algorithm for MNFC suspensions was previously discussed.[11] It is only

Table I. Composite Suspensions Nomenclature, Where Material Content is Expressed as Percentage by Weight of Total Formulation

Samples used for the study	
Consistency/%	SAMPLE NAME =consistency %amount of fibrillated material %type of fibrillated material + 70% PCC filler + 100 – other constituents as fibres %
5	5% 20% MFC (10% fibre 20% MFC 70% PCC)
	5% 30% MFC (0% fibre 30% MFC 70% PCC)
	5% 20% NFC (10% fibre 20% NFC 70% PCC)
	5% 30% NFC (0% fibre 30% NFC 70% PCC)
10	10% 20% MFC (10% fibre 20% MFC 70% PCC)
	10% 30% MFC (0% fibre 30% MFC 70% PCC)
	10% 20% NFC (10% fibre 20% NFC 70% PCC)
	10% 30% NFC (0% fibre 30% NFC 70% PCC)
15	15% 20% MFC (10% fibre 20% MFC 70% PCC)
	15% 30% MFC (0% fibre 30% MFC 70% PCC)
	15% 20% NFC (10% fibre 20% NFC 70% PCC)
	15% 30% NFC (0% fibre 30% NFC 70% PCC)

possible to correct for a non-linear flow profile in the vane-in-cup device when the measuring protocol and suspension consistency (solids content) provide a clearly defined determination of yield stress (τ_0), without giving rise to otherwise unpredictable rheological behaviour.[14] Most analyses of the rheological properties of MFC/NFC-composite suspensions follow the classical demand of rheometry, that is, equilibrium viscosity conditions under long-time shear. However, many envisaged industrial applications involve transient flow environments, and the final consolidation of a complex composite is often occurring under extended low shear conditions. Additionally, many industrial current and proposed applications of MFC/NFC include the development of nanocomposite structures derived from dewatered bulk suspensions.

Under static or low shear conditions, gel structures may exhibit very different rheological behaviour depending on the mechanism of gelation.[15–18] In the case of high aspect ratio rod-like particulate nanofibrillated cellulose, a similar water trapping mechanism constructs the gel, and the application of strain under low shear for continued periods can lead to structure ensemble orientation.[19–22] The strong mutual Coulombic repellance of the highly charge nanoparticles and the immobilisation of the trapped interstitial water act together to create highly elastic structured zones, similar in behaviour to those found in liquid-crystalline materials.[21–24] As the particulate length increases, the axially orientated rotation slows and becomes limited with retained layered direction.[25] For industrial application of complex high consistency MNFC-composite suspensions it is essential to understand the rheological behaviour during the regime of solids content increase, that is, during dewatering.

Incorporation of shear rotation in order to shear-thin the viscoelastic structure under vacuum, enables the structure-water-retention property relation to be established.[26,27] Therefore, we refer to previously analysed rheological structure data using the immobilisation cell (IMC) which enables possibility of designing intervals of shear and oscillation toward equilibrium dewatered state, to determine the Weissenberg normal deformation of the parallel plate geometry and relate this to the novel strain-induced low shear structure in the cylindrical vane-in-cup geometry.[28–30] Because of the likely banding within the strained gel, the superposed structuration, manifested here as observed rheopexy, is considered to result in regions of a semi-ordered or quasi liquid-crystalline state.[31–33]

EXPERIMENTAL

Material and Methods

The wood fibre pulp, acting as the carrier extender for the MFC/NFC and pigment filler composites, consists of pressure ground bleached pine softwood (pw). The filler used in the composite suspensions was a commercial undispersed precipitated calcium carbonate with scalenohedral morphology (SPCC) supplied by Omya AG, Switzerland.

NFC/MFC Production

Two types of nanocellulose containing materials were used, microfibrillated cellulose (MFC) and nanofibrillated cellulose (NFC). MFC was produced from never-dried bleached Birch Kraft pulp. The fibrillation was carried out by passing the pulp three times, at 3% solids, through a Supermasscolloider grinder (Masuko Supermasscolloider, MKZA 10-15) equipped with SiC grinding stones (MKE10-46 Masuko Sangyo). The material had a turbidity transmittance of 34% at 0.1% consistency (solids content) at a wavelength of 800 nm. The applied NFC sample was a semi-commercial one, produced with the TEMPO-oxidation process from never dried birch pulp. Following oxidation, the material was treated by a single pass through a fluidiser (Microfluidics M700, Microfluidcs, Newton, MA). Carboxylic acid content on the NFC was 0.1 mmol/g determined by conductometric titration. The NFC had a degree of substitution of 0.2 and was prepared at 2.3% consistency. Descriptions of the materials used and their properties are presented in Table I. The Brookfield (vane) viscosity at 10/min (rpm) of 1.5% solids MFC was 23 000 mPas, and for NFC samples of 1.5% solids it was 46 657 mPas.

NFC/MFC Topological Properties by Atomic Force Microscopy (AFM)

Nano-scale topology of disintegrated MFC and NFC/TEMPO-oxidised nanofibrils was investigated using a Nanoscope IIIa

Table II. Description of Materials Used for MNFC-Suspensions/Composite Furnishes and Their Properties

Particle	pH	Particle/Agglomerate size	Zeta potential ζ/mV
SPCC	9.0	4.3 μm	−9.8
MFC 3 pass Birch Kraft pulp	9.5	6.6 μm	−24.3
NFC TEMPO-oxidation	8.9	977 nm	−57.0
pw bleached softwood pine	8.8	(SR 24)[a]	−15.0

[a] "SR" refers to the Schopper-Riegler value of the fibre pulp.

Multimode scanning probe microscope (Digital Instruments, Santa Barbara, CA). The images were scanned using silicon cantilevers (Ultrasharp μmasch, Tallinn, Estonia). The MFC/NFC samples were diluted with MilliQ-water to 100× dilution. A droplet of the diluted solution was then placed on a mica surface, and the droplet was allowed to dry before the AFM investigation. No image processing was undertaken except image flattening. The fibril dimension analyses were carried out by Nanoscope Analysis software (Version 1.5, Bruker) employing the section tool. At least 10 different sections from separate MFC and NFC fibrils of each image were analyzed.

NFC/MFC Containing Suspensions

Suspensions of cellulose fibres and the nanofibrillated samples, containing either NFC or MFC, were prepared for individual analysis at four different concentrations (1.0%, 1.5%, 2.0%, and 2.3%, respectively). Different consistency MFC and NFC suspensions were obtained by dilution of initial stock concentrations of 3.0% and 2.3%, respectively. Dilutions were made using de-ionized water. The suspensions are labelled according to their consistency and type in respect to material content (MFC/NFC). The final pH of all suspensions was between 8.0 and 8.2.

MFC/NFC-Pigment Composite Suspensions

The composite furnish described here is specially designed with unusually high levels of filler as part of the development of composites including MFC/NFC as a strengthening aid,[28,29] allowing the use of exceptionally high filler loading enabling the replacement of a portion of the cellulose fibres, Table I.

The pigment was added after adjusting MFC/NFC consistency, and mixed for 1 h in a Diaf mixer (Pilvad Diaf A/S, Denmark), after which the cellulose pulp was added with further mixing under the same conditions. De-ionised water with pH 8.1 and conductivity 0.5 μS was used for the suspension make-down and for adjusting solids consistency of composite suspensions.

Characterization of NFC/MFC-Containing Composite Suspensions

Zeta potential (ζ) was determined by measuring electrophoretic mobility of pigments, MFC and NFC with a Zetasizer Nano ZS series (Malvern Instruments, Worcestershire, UK), measuring the velocity of the particles using laser Doppler velocimetry. The average particle size of the pigments, MFC and NFC was measured with dynamic light scattering (DLS), using photon correlation spectroscopy (Malvern Instruments, Worcestershire, UK). Before measuring ζ and ensemble average particle size, the samples were diluted with de-ionised water to a solid content of 0.01 w/w. Characterisation of materials used in MNFC furnishes is presented in Table II.

Rheometry

Oscillatory Measurements. A rotational and oscillation rheometer (Physica MCR-300) was used in both controlled shear and strain modes with a plate-plate geometry. The rheometer was equipped with roughened (serrated) top (PP20) and bottom (P-PTD 200) plates, the bottom one also implementing a Peltier temperature control, with temperature fixed at 23°C. The gap was initialized to 1.5 mm. Both MFC/NFC suspensions and composite furnishes containing them were measured applying a strain sweep followed by a frequency sweep in the linear viscoelastic (LVE) region, predetermined by a strain-

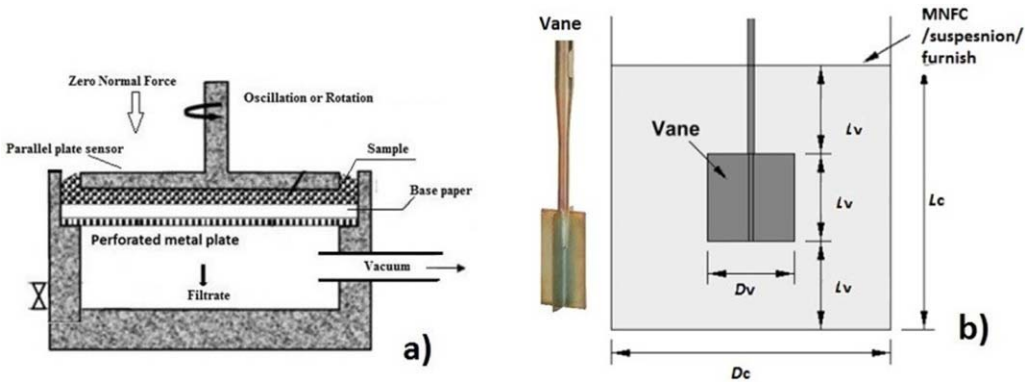

Figure 1. Schematic showing the measurement devices applied in this research: (a) immobilisation cell (IMC) as attached to the MCR 300 rheometer and (b) wide gap Brookfield viscometer with vane-in-cup geometry. [Color figure can be viewed in the online issue, which is available at wileyonlinelibrary.com.]

Table III. Oscillation-Shear Cycle Scheme

	DSO phase ($\gamma = 0.1\%$, $\omega = 10$ (rad)/s)				CSR phase ($\dot{\gamma} =$ 0/10/s)		
Interval number	1	2	9	10	11	12	13
Cycle phase	DSO	CSR	DSO	CSR	DSO	CSR	DSO
Interval duration/s	100	10	100	10	100	10	100

amplitude sweep at a constant angular frequency (ω) of 10 rad/s. In the strain sweep, the strain (γ) was varied between 0.1 and 500%.

Oscillation-Shear Cycle Viscoelastic Structure Formation (Plate–Plate). Complex systems, as described by the materials used in this study, undergo multiple structural configurations including and generating a variety of elastic interactions.[34–36] This is reflected using a Physica MCR 300 rheometer with an immobilisation cell (IMC) accessory, as licensed from BASF AG, Figure 1(a). This special device is normally used for dynamic dewatering studies, but here, instead of following the dewatering process, the built-in gap change monitoring facility is used for recording the Weissenberg normal force-induced gap increase when applying instantaneous continuous shear (CSR) following a period of direct low strain oscillation (DSO), during which the quasi-static viscoelastic structure build-up has taken place within the linear viscoelastic region. A parallel plate geometry measuring system (PP-50) with 50 mm diameter is used throughout. The samples were pre-sheared prior to the first DSO interval for 100 s, with shear rate $\dot{\gamma} = 10$/s, at a minimum share rate to ensure break down of static or other structures and then the periodic succession of DSO and CSR proceeded, as presented in Table III. Using this device in the novel manner described, we can identify the elastic structure formation by observing the time dependant gap increase, and by analysing the rate of change in gap at the start-up of the shear phase, we can parametrize the Weissenberg response.

In this experiment, the samples have been equilibrium dewatered and so brought to the point in each case where the internal static structure will be highest. We then compare the Weissenberg response measured in this way, providing a measure of static structure, with the time constant of low shear structuration described below to establish whether there is a correlation or otherwise, between the two mechanisms structure build.

Brookfield Wide Gap – Vane-In-Cup. The wide gap vane-in-cup cylinder geometry was chosen for determination of flow curves outside the controlled LVE region, thus complementing

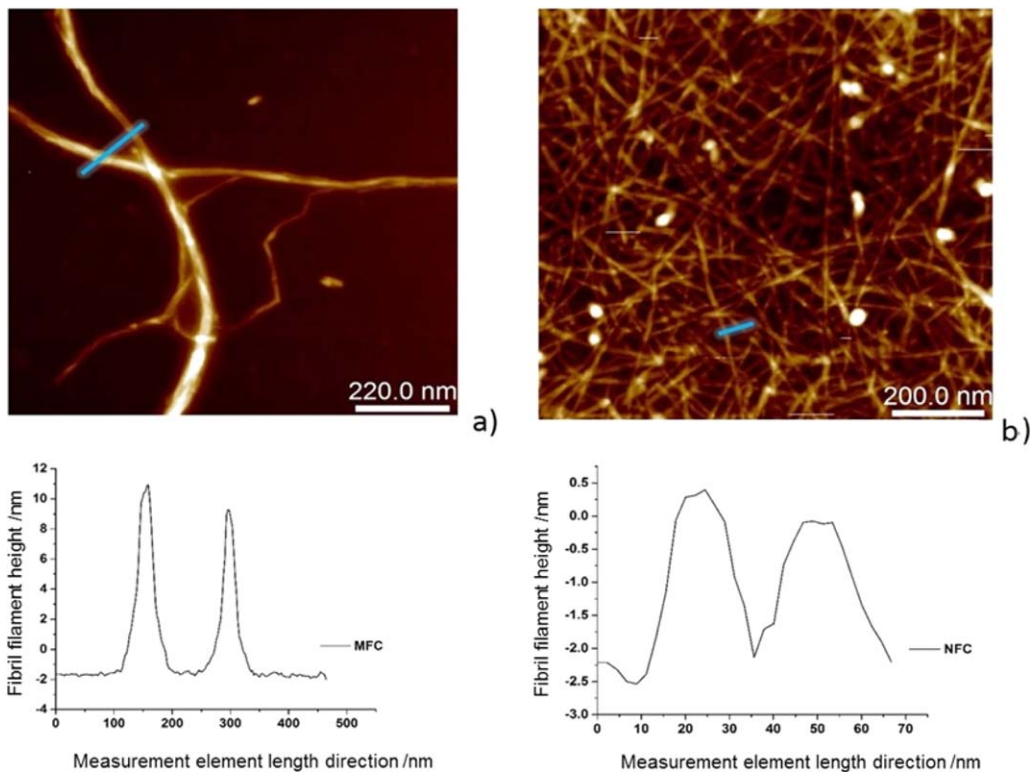

Figure 2. Example analysis of fibril diameter (height) by AFM (in air): (a) MFC and (b) NFC fibrils. For imaging, the fibrils were previously deposited on a mica substrate. In the 2 x 2 μm^2 images the blue lines connecting two fibrils represent the measurement directions from where the height profiles were plotted. [Color figure can be viewed in the online issue, which is available at wileyonlinelibrary.com.]

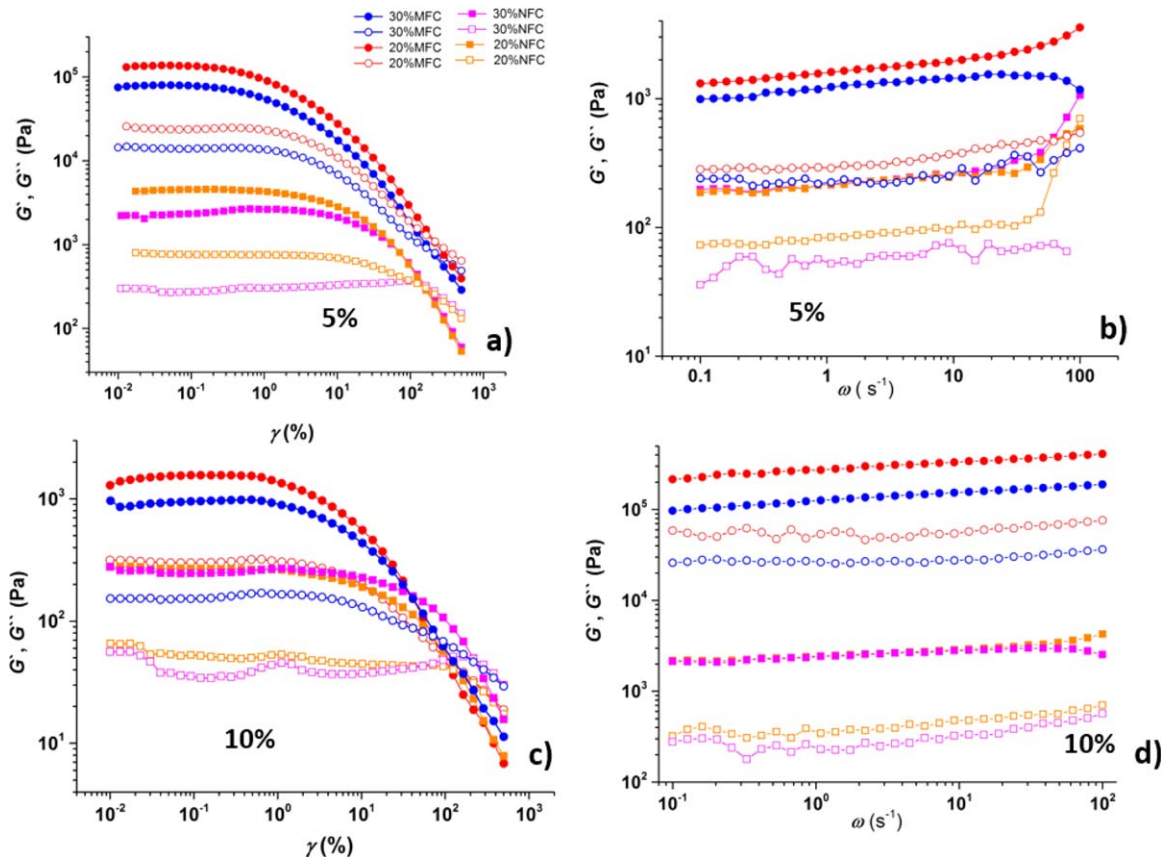

Figure 3. Oscillatory measurements: G' and G'' taken from (a) amplitude sweep for 5% composite suspensions, (b) frequency sweep for the 5% composite suspensions, (c) amplitude sweep applied to 15% composite suspensions, (d) frequency sweep 15% composite suspensions. [Color figure can be viewed in the online issue, which is available at wileyonlinelibrary.com.]

the plate-plate geometry and gap change rate analysis.[11] The apparent low shear viscosity was determined (Brookfield DV-II+) adopting the four bladed vane viscosity units V-73 ($D_v = 0.587$ cm and $L_v = 1.176$ cm) and V-74 ($D_v = 0.587$ cm and $L_v = 1.176$ cm), Figure 1(b). The vanes were applied according to the MNFC type and consistency, as V-73 for MFC 1% and 1.5% suspensions and V-74 for the remaining samples. Furthermore, wall slip, apparent and real, is effectively avoided by the combination of vane geometry and a wide gap.

The MNFC suspension/composite suspensions were poured into the cylindrical glass cup cell of 200 cm^3 capacity with a diameter of 6 cm, as described in an earlier publication.[11] The measurement protocol was defined with the computer software Lab Weg connected to the viscometer. To ensure that the strain accumulated due to the high thixotropy of such materials during loading into the glass cell has no influence, the samples were each time pre-sheared for 2 min at 200 min^{-1} (rpm). To measure the dynamic flow curve, we increased the rotation rate in five interval steps, with logarithmic spread of measuring points by applying a sequence of rotation speeds (Ω) of 0.5, 5, 10, 50, and 100 min^{-1} with 5 min measuring time at each interval. Measurements were repeated five times each, including the pre-shear protocol. The shear stress τ inside a concentric cylinder rheometer is given by

$$\tau = \frac{M}{2\pi h\left(\frac{D_c - D_v}{2}\right)^2} \quad (1)$$

where the parameters follow the nomenclature in Figure 1(b), namely h ($=L_v$ in the case of the vane geometry) is the height of the rotating cylinder length, D_c the diameter of the outer cup, D_v the diameter of the shear element (vane in this case) and M is the applied torque in mN/m, calculated from known values of the viscometer torque reading, T(%), given from the viscometer in % of the maximum machine torque, which for the Brookfield DV-II+ is $M_{max} = 0.7187$ mN/m ($M = TM_{max}/100$). From this equation, as discussed in our previous publication, the shear stress at the glass cell wall is around 1–4% of the value at the spindle edges.[11] Shear rates calculated according to the Brookfield manual can be obtained by

$$\dot{\gamma} = \tau/\eta = 100Ts/\Omega \quad (2)$$

where τ (Pa) is given by Eq. (1) and η (Pas) is the viscosity and T(%) is the viscometer torque reading in percent, Ω the rotation frequency (min^{-1}) value and s is the ratio of the Stress Multiplier constant (SMC) and shear rate constant (SRC), given by the Brookfield manual and depending on the dimensions of the vane spindle. The normal gap assumption made when calculating the shear rate in a concentric cylinder viscometer is not sufficient when complex fluids are considered, and it is necessary to take the spatial heterogeneity into

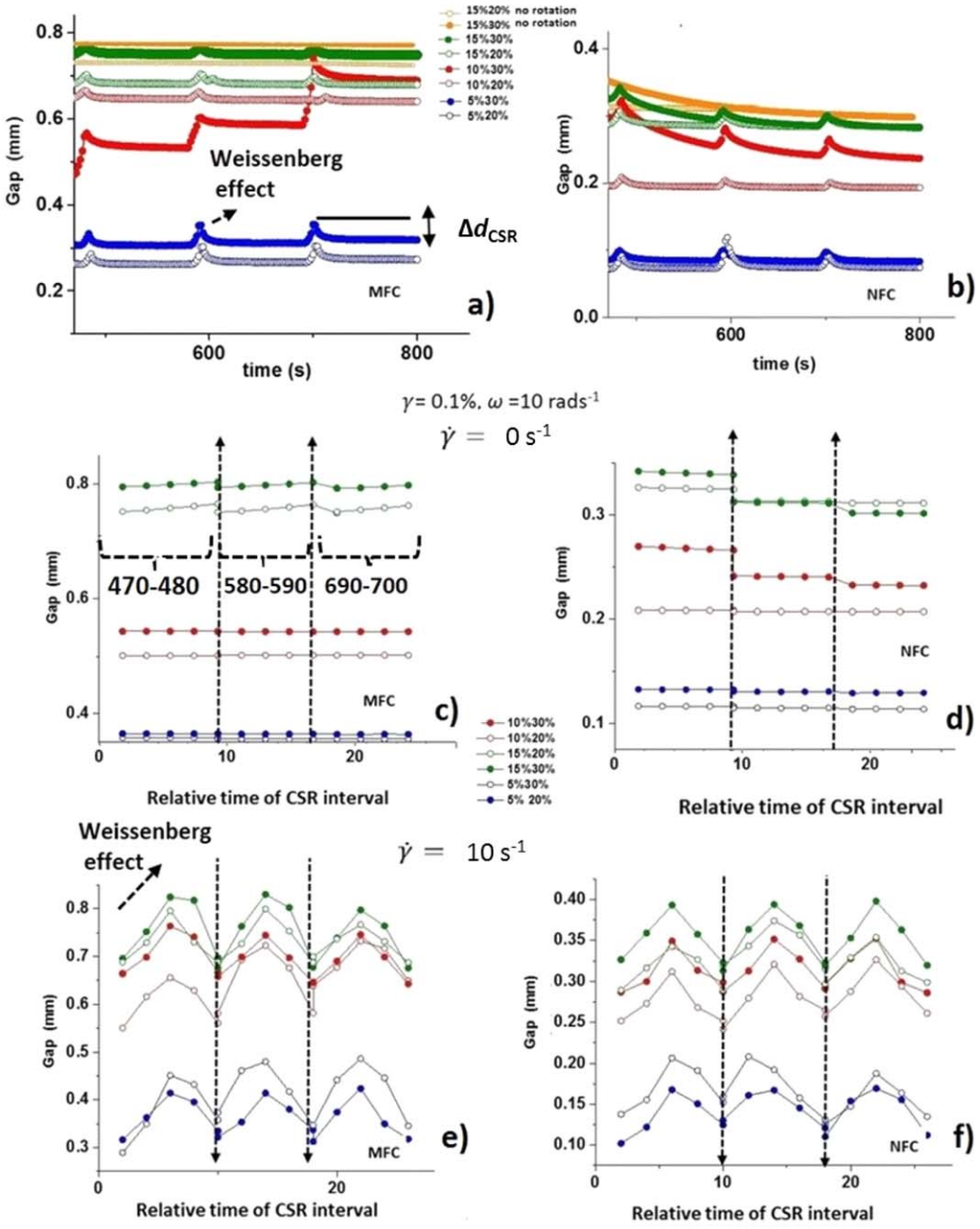

Figure 4. Gap behaviour at IMC oscillation (DSO)/rotation/(CSR) scheme that monitors changes in sample dimensions in the direction normal to shear. Gap behaviour at last three CSR and DSO intervals (8–13 intervals) for (a) MFC and (b) NFC composite furnishes, respectively. Absence of changes in sample dimensions during last three CSR intervals (8, 10, and 12), without application of shear ($\dot{\gamma} = 0$/s) between vacuum intervals for (c) MFC and (d) NFC composite formulations respectively, and when shear is applied ($\dot{\gamma} = 10$/s) last three CSR intervals (8, 10, and 12), (e) MFC and (f) NFC composite formulations, respectively. [Color figure can be viewed in the online issue, which is available at wileyonlinelibrary.com.]

account. For materials having high yield stress, as exemplified by MNFC-composite suspensions, a derivative method has been proposed, in which shear rate at the vane spindle is given by

$$\dot{\gamma}(M) = \sum_{p=0}^{\infty} \left[2M \left(\frac{D_v}{D_c} \right)^p \frac{\delta\Omega}{\delta M} \right] \left(M \left(\frac{D_v^2}{D_c^2} \right)^p \right) \quad (3)$$

where p describes the numerical derivative series elements.[11,13]

For high consistency complex fluids using the geometries described here, the Brookfield viscometer frequently suffers from torque overload, that is, the maximum machine torque is easily exceeded $T_{max} = 100\%$, and so it is not possible to use the simplistic assumptions implicit in Eq. (3) across the whole measurement time. However, it is this very limitation that has led to the novel analysis proposed in this work to be able to establish a time constant for shear thickening

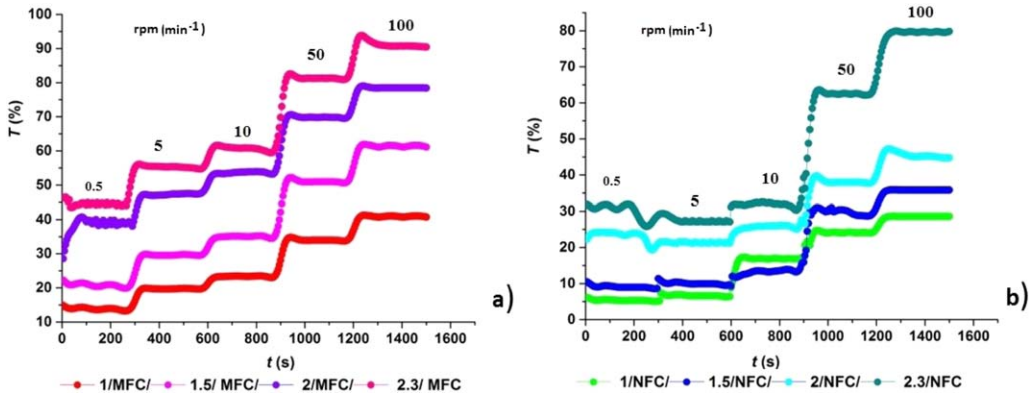

Figure 5. Vane-in-cup geometry torque T(%) (given as a percentage of maximum rotor torque for Brookfield DVII + viscometer = 0.7187 mN.m) response for different Ω (rpm = 0.5, 5, 10, 50, and 100 min^{-1}): (a) MFC suspensions, (b) NFC suspensions. [Color figure can be viewed in the online issue, which is available at wileyonlinelibrary.com.]

phenomena. The rate of the continuous low shear-induced viscosity increase with time (rheopexy) is characterized and used to derive a gel structure alignment time constant, which we relate to the Weissenberg plate–plate separation observed at the IMC upon start-up of each of the rotation (CSR) intervals, following a given solids increase during vacuum applied intervals (DSO).

Rheological Data Processing and Reproducibility. For the complex high consistency composite suspensions measured here, containing in their matrix mix fillers and thixotropic gel-like MNFC particles, the data variation of the rheometrical measurements (plate–plate IMC rheometer and Brookfield viscometer) was within ±5–7%. This is considered acceptable considering the sample complexity including structuration and gelation. Rheological data involving gel-like MNFC, contained mechanical noise, which, unless stated otherwise, was subsequently smoothed by Tikhonov regularisation.[29,37]

RESULTS AND DISCUSSION

Atomic Force Microscopy Observations

The results for the size properties obtained with AFM are in good accordance with previous characterisations both for MNFC.[8,34] In Figure 2, the MFC fibrils have clearly larger dimensions than those of NFC. NFC particles are straight and rod-like with reduced length in comparison with the longer somewhat flexible MFC. The AFM height profiles for low charged mechanically disintegrated MFC report a typical single fibril diameter to be in the range 9–12 nm, for example, Figure 2(a), whereas the highly charged NFC is smaller, being in range 2–3 nm, for example, Figure 2(b).

Rheometry

Oscillatory Measurements (Plate-Plate Geometry). As expected, for all MFC and NFC suspensions and MFC/NFC-containing furnishes, the G' and G'' moduli increase with consistency.

Figure 3 presents G' and G'' MFC/NFC furnishes, from amplitude sweep and frequency sweep measurements, respectively, for 5% Figure 3(a,b), and for 15% MNFC composite suspensions, Figure 3(c,d). The presence of pulp fibres, which have lower ζ than MNFC (Table II) decreases the zeta potential of furnishes, which results in flocculation between components seen as an increase of G' for MFC over NFC-composite suspensions.[10,29,30,36] Data obtained from the amplitude sweep measurement presented in Figure 3(a,b) show that MFC-containing composite suspensions for both 5% and 15% consistency have higher G' than the ones based on NFC, including a longer strain span showing linear viscoelastic response (LVE), that is, before the decrease of G' as a function of strain. That the decrease of G' in the case of NFC in these complex suspensions occurs at lower strains than in case of the MFC-based suspensions can be reconciled with the shorter fibrillar length of the NFC and so there is less opportunity provided for long range entanglement to occur. Furthermore, this view is supported in that the G' is higher for complex suspensions that contain cellulose fibres, which have even longer fibres and as a result even greater entanglement especially as a function of increasing solids content Figure 3(b–d) display the response of dynamic moduli G' and G'' of the composite suspensions as a function of oscillation frequency. The G' and G'' of the low consistency 5% composite suspensions are virtually independent of frequency, as they are at a very low level, while the medium range consistencies are strongly dependent. This behaviour is typical of a transition from a weak-gel structure at low consistency to a medium-strong gel structure as consistency increases. In Figure 3(d) shows the case of the strongest gel structure where both G' and G' remain high throughout the whole frequency range.[29]

Oscillation-Shear Cycle Viscoelastic Structure Formation (Plate-Plate). The gap change data, plotted in Figure 4, depict the dewatered equilibrium state in respect to sample volume. The final position at which the gap becomes constant is lower for the NFC- than MFC-composite suspensions, related to compaction within matrix.[28,35,36] Of interest to the current research here is the gap behaviour during the start-up of the rotation intervals (CSR), which shows markedly significant gap increase points at the beginning of each rotation cycle, due to the response of the highly viscoelastic structure formed during relaxation in the DSO interval.[38,39] This response leads to a normal force, Weissenberg effect, and hence the action of separating the plates as was observed, but not analyzed, in a

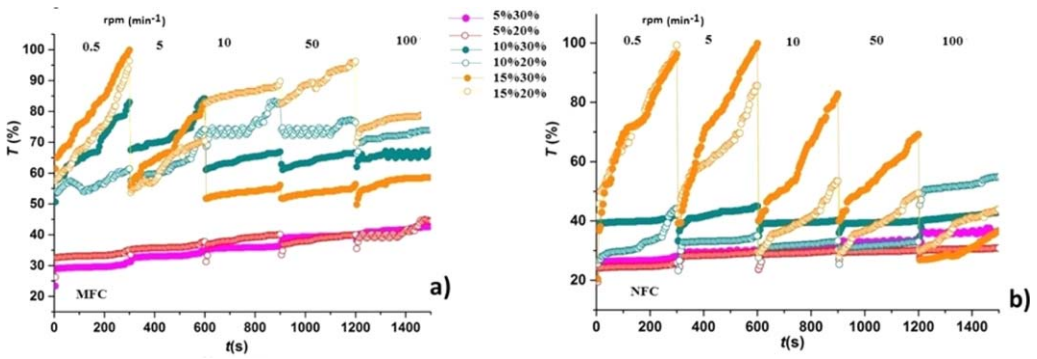

Figure 6. Vane-in-cup geometry torque $T(\%)$ response for different Ω (rpm = 0.5, 5, 10, 50, and 100 min^{-1}) for 5, 10, and 15% consistency composite suspensions, respectively: (a) MFC-composite suspensions, (b) NFC-composite suspensions. [Color figure can be viewed in the online issue, which is available at wileyonlinelibrary.com.]

previous publication, in which, for comparison purposes, we chose to follow the increase in η^* (DSO) and change in η (CSR) to study dewatering kinetics.[28] Figure 4(b–d) compare the change in filtered sample volume for 10% consistency composite suspensions, containing 30% NFC and MFC, respectively, expressed as difference in gap position, with the increase in consistency during dewatering expressed as the change in η during the CSR intervals. Shear thinning after each Weissenberg episode at start-up of shear application subsides and to a smaller extent depending on the deformation during the DSO vacuum interval, as well as the many various internal viscoelastic factors, which also change with the solids content. The Weissenberg effect is present to different extents upon start-up of the shear intervals for the various furnishes, as presented in Figure 4(b–d), throughout the whole measurement. For clarity we choose to show furnishes without pulp fibers, but very similar behaviour is observed with the presence of pulp fibres. In order to provide more detailed insight into the presence and nature of the Weissenberg effect upon shearing, gap decrease diagrams are plotted over a concentrated timescale interval, Figure 4(c,d) during which there is a marked increase of gap during the shear interval. This is then expressed as the gap increase, Δd_{CSR}, at the start of each CSR region occurring over the time interval Δt, namely, $\Delta d_{CSR}/\Delta t$.

Wide Gap Vane-In-Cup Viscometry. The shear stress inside the concentric cylinder rheometer is given above in Eq. (1). The stress at the cup edge is implicitly expected to be below both the yield stress and below the onset stress for wall-slip. Since this study records increasing stress with continued shear, we

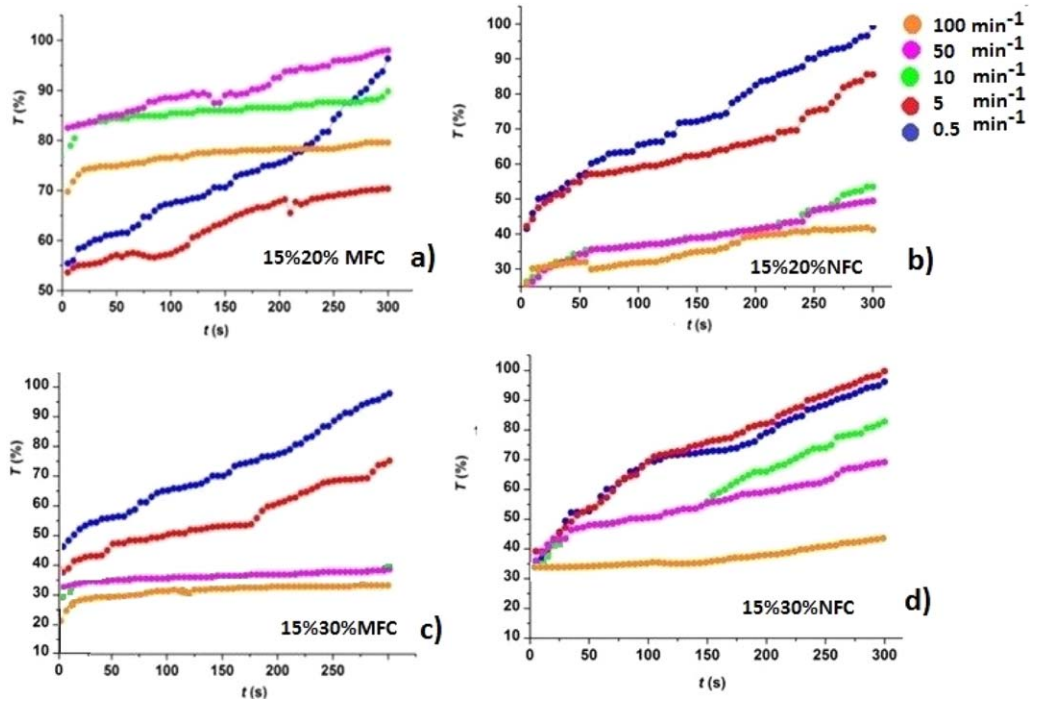

Figure 7. Vane-in-cup torque T (%) response for Ω = const. as a function of time for: (a) 15% MFC composite suspensions and (b) 15% NFC composite suspensions, with cellulose fibres, and (c) 15% NFC composite suspensions, and (d) 15% NFC composite suspensions, without cellulose fibres, respectively. [Color figure can be viewed in the online issue, which is available at wileyonlinelibrary.com.]

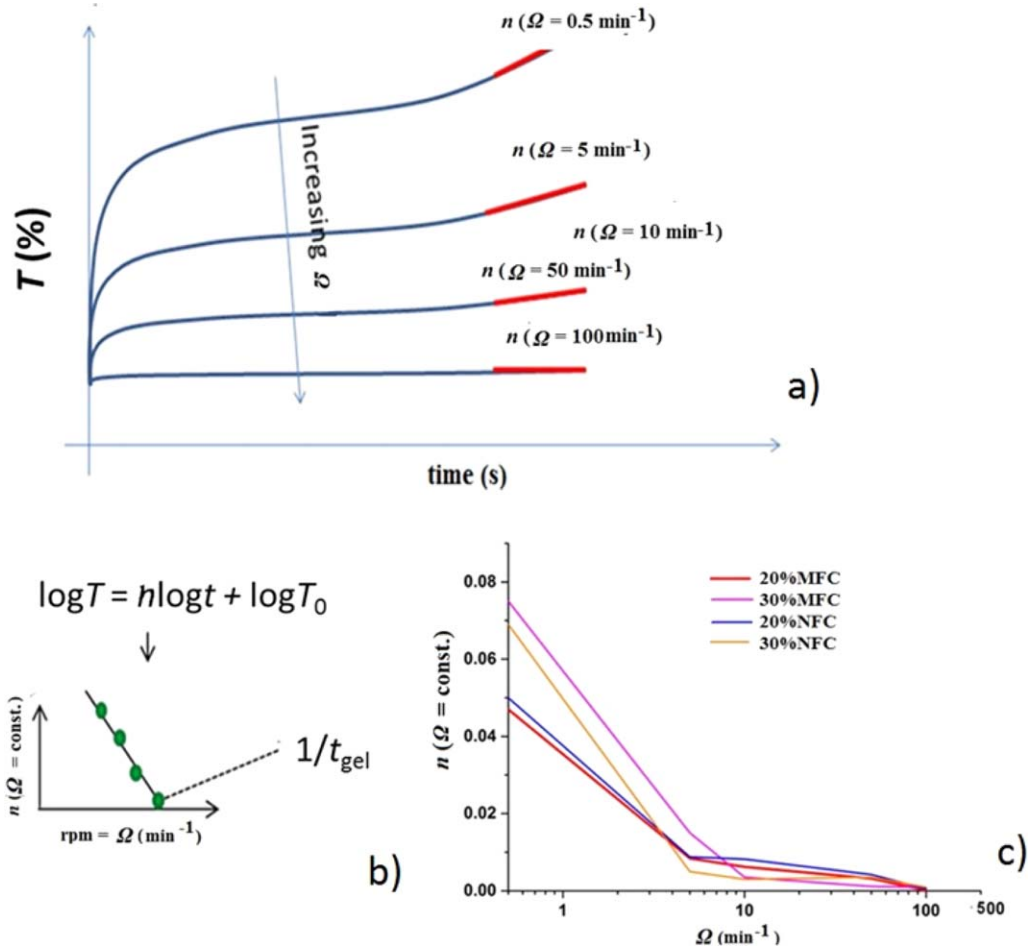

Figure 8. (a) Schematic presentation of extrapolation of torque (T) curves over a range of constant shear rates (Ω = rpm = 0.5, 5, 10, 50, and 100 min^{-1} showing determination of the power law coefficient (n) for developed rheopectic behaviour of the suspension flow curves using data from 200–300 s of continuous shear, (b) the explanation decrease of power law coefficient (n) with increase of Ω for a given consistency, and (c) the coefficient descriptor for rheopexy, n, for composite suspensions as a function of Ω, calculated after extensive shear at each of a series of constant Ω. [Color figure can be viewed in the online issue, which is available at wileyonlinelibrary.com.]

conclude that, at least to a first approximation, this assumption holds true. The non-linear profile of the material flow curves is presented as torque (T) dependence on the corresponding radial velocities [Ω = rpm (min^{-1})], given as % value of maximum spring torque for the Brookfield DV-II+ viscometer, and readily shows the limitations of this measuring device for high consistency suspensions, that is, for 15% composite furnishes, T lies at ~100%. In Figure 5(a,b) the low shear experiments are conducted for MFC/NFC suspensions at all the different concentrations. We see more or less stable behaviour of MNFC suspensions during measuring time for each given shear rate. T increases with increase of Ω, with stable behaviour of $T(\Omega)$ for given Ω.

The eventual steady state behaviour of MFC/NFC suspensions can be found in the up and down shear rate sweeps, discussed in our previous publication.[11] In the case of furnishes, however, the response of stress is not stable over time during the periods of analysis studied here, with irregularities in flow curves being stronger for high consistency composite furnishes. The more complex behaviour of high consistency MNFC-composite suspensions, presented in Figure 6(a,b), for the same measuring protocol as in Figure 5, shows that raising the consistency of MFC/NFC-composite suspensions increases water retention in the particle interstices and increases the work that would be needed to be done to overcome rheopexy.[16,17]As presented in Figure 6(a) for NFC-composite suspensions, there are large differences in the rheopectic behaviour in respect to solids content/consistency, rather than simply the presence of cellulose fibres in the composite suspension matrix and Figure 6(b) shows the similar for MFC-composite suspensions. For all MNFC-composite suspensions, we see a very steep increase of torque toward a maximum value at the end of the rotation interval: T increases to a maximum of 100%, which makes it impossible to perform further measurement toward reaching any potential steady state. The torque evolution as a function of time is similar to strain hardening in gel forms, rhepectic behaviour suggests some sort of development of fibre–fibre structure, acting to trap interstitial water making it unavailable for further flow, that is, the formation of "dead zones" between

Table IV. Time Constant of Strain-Induced Superposed Structuration, t_{gel}, [Eq. (5) for MFC/NFC-Composite Suspensions, Showing Vane-In-Cup RPM and Shear Rate Eq. (2)].

	Ω (rpm) at which $n = 0$ (min^{-1})			
Composite consistency (%)	20MFC	30%MFC	20%NFC	30%NFC
5	100	110	115	130
10	200	400	400	480
15	650	650	600	700
	$t_{gel}(n = 0) = 1/\dot{\gamma}$(ms)			
5	45.0	41.2	40.9	34.0
10	22.7	11.4	11.4	9.9
15	7.1	7.1	7.5	6.5

collective fibre alignments, similar to quasi liquid-crystalline-like structures.[13,17] Higher consistencies, 10% and 15%, show that rheopexy is decreasing non-linearly with progressive increase in shear rate, Figure 6. This indicates the presence of a characteristic time constant of the rheopectic effect for each respective composite suspensions mix.

Figure 7, in turn, presents torque development for furnish compositions for the 10% and 15% consistencies of MFC and NFC-composite suspensions at constant Ω. In Figure 7(a,b) are composite suspensions which have cellulose fibres present in the furnish matrix (20% MFC/NFC), whereas in Figure 7(c,d) are composite suspensions that have NFC only within the composite (30% NFC). Evident to see is similar form of development of $T(\Omega)$ for the different consistencies regardless of the presence of cellulose fibres in the furnish. As seen in Figures 6 and 7, evolution of T is greater at low Ω and higher consistencies. Thus, we can conclude that if the sample is sheared at a rate higher than the time constant in the superposed gel structuration, then the torque remains constant without any induced rheopexy, that is, the rate of stirring breakdown equals or exceeds the rate of structure formation. As also presented in Figure 7 at higher consistency, the structure is retained and requires higher energy input to destroy its integrity progressively. This dependency on consistency is important in practical application systems with MNFC and fibrous structures, which can undergo superposed strain-induced structuration, which in turn defines the end-product structural orientation.[32,33]

Time Constant of Structuration

To extract the time constant described above, it is necessary to characterise the rate of rheopectic viscosity growth as a function of time. Without implying any power law-related mechanism, it is nonetheless convenient to parameterise this growth rate locally by a simplistic first order power law expression. By fitting the time evolution of torque, $T(t)$, in this way, we can derive a characteristic parameter $n = f(\Omega)$ for a series of rotation rates, expressed as a function of frequency

$$T(t) = T_0 t^{n=f(\Omega)} \quad (4)$$

where T_0 expresses the plateau value before the secondary rheopexy. Using Eqs. (1 and 2) it is possible for a given vane-in-cup geometry to give an estimation of the T and Ω, respectively, at which the structure time constant is in equilibrium with the frequency of rotation, i.e., Ω, obtained by extrapolating to the Ω at which the parameter reaches zero. This is the only possible approach since the system is not in the steady state, i.e., it is not possible to apply Eq. (3). By using this novel approach, a valuable new parameter can be obtained describing the time constant of the transient state, and so making the method applicable to a much wider range of application conditions in the real world of industry where long term stirring is a regular process or storage procedure. By making the extrapolation described above to the value of rpm, Ω, (or $\dot{\gamma}$ derived from it) at which $n = 0$ where the rotation rate is in unstable equilibrium with the gel formation constant, t_{gel}, we obtain

$$\dot{\gamma}_{n=0} = 1/t_{gel} \quad (5)$$

A schematic representation of the method above is presented in Figure 8(a), in which we parameterise and extrapolate the power law coefficients (n) obtained from the flow curves of all composite suspensions (as presented for 10% and 15% in Figure 8) for the last 200 s of the Ω = const. interval. This enables us to capture the rheopectic torque evolution, and in particular its decrease upon increase of shear rate for each given composite suspension. Development of torque, T, indicates the stress

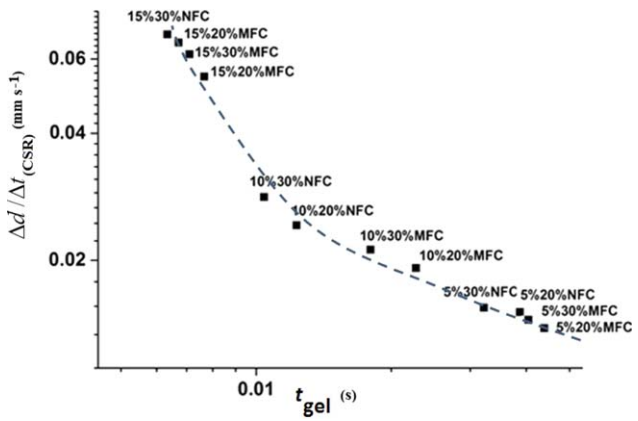

Figure 9. Correlation between Weissenberg behavior, expressed as average value of relative gap increase gradient upon start-up of shearing (CSR), $\Delta d_{CSR}/\Delta t$, during IMC oscillation-shear intervals under plate-plate geometry, and superposed low shear structuration in respect to induced structure orientation (t_{gel}), presented in Table IV. [Color figure can be viewed in the online issue, which is available at wileyonlinelibrary.com.]

development effect in the suspension, and the rheopectic behaviour can be expressed as the descriptor *n*. The characteristic decrease in *n* as a function of Ω describes the structure time constant in respect to the intercept with the Ω axis. Figure 8(b,c) display the extrapolation plots for the descriptor *n* as a function of the Ω.

In Figure 8, we see that the step between the various Ω (rpm) values leads to discontinuous curves, but this does not affect the end result being sought after. Of further interest, however, is the nature of the breakdown of some of the induced structures exemplified as higher shear is applied.[40] Similar phenomena have also been reported for coalescence coupling with flocculation in the case of dilute emulsions.[41,42] The time constant data for strain-induced superposed structural orientation are shown in Table IV.

The breakdown of orientational shear-induced structures under increased shear is considered to be hierarchical, suggesting at least a two-level hierarchy in some cases, which should in further research be observed with rheo-optical or neutron scattering experiments, depending on solids content.

Correlating Weissenberg Effect with Gel Structure Hardening at Low Shear. To highlight the relation between the strain-induced structure development behaviour of high consistency NFC/MFC composite formulations, we correlate the Weissenberg effect in IMC during successive oscillation-rotation intervals using plate-plate geometry, with that of torque (T) increase, and hence t_{gel}, in vane-in-cup geometry. Figure 9 presents the correlation curve of the calculated average value of gap increase during CSR intervals (Table III) for each composite furnish, Figure 4, with the strain-induced superposed structuration formation time t_{gel} presented in Eq. (5) and Table IV. That this value of $\Delta d_{CSR}/\Delta t$ (on the IMC) is on average constant within each formulation during the instantaneous application of shear after elastic structure formation during DSO intervals, shows that the elastic structure strength build is uniform at the point of highest internal static structure. The structure build probably involves some self-assembly mechanism rather than a random entanglement, and the correlation with the time constant for rheopectic viscosity increase (Brookfield vane) under continued low to moderate shear supports a similarity between the two structure-forming regimes, that is, that observed during low strain and that of an oriented mesophase liquid crystal-like behaviour. At large shear-induced hardening time constant, $t_{gel} \gg 10$ ms, we see that the static structure (Weissenberg effect) contributes little to the strain hardening effect, but at $t_{gel} < 10$ ms the elastic static structure can be assumed to contribute, and maybe act as an initiator to the strain hardening observed after prolonged low shear. Clearly, there lies important information in studying such coupling effects.

CONCLUSIONS

Strain-induced structures are ubiquitous among high aspect ratio nanomaterials, and especially prevalent in combination with micro and nanofibrillar components. MFC/NFC-composite suspensions are expected to be no exception. Such structures are similar to quasi liquid-crystal-like domains, and are induced under consistent extended low to medium shear application, typically in the presence of likely shear banding. The study outlined in this article undertakes to describe the viscoelastic properties of high consistency composite suspensions containing micro and nanofibrillated cellulose (MFC/NFC), and in particular their strain/shear induced structure properties. The potential of parameterising the rheopectic quasi gel hardening structuration development is highlighted in a novel data analysis method. Parameterising the viscosity increase as a function of time in terms of a simple descriptor over a range of shear rate enables the dynamics of structure development to be defined as a time constant, t_{gel}, which expresses the superposed structuration in terms of an ensemble domain orientation rate of high aspect ratio materials under constant low shear. The dynamics of the ensemble interactions can thus be determined, which are critical for describing the transient properties of such micro and nanomaterials under industrial forming applications. The principles presented in this work can be applied to many transient phenomena of particulate suspensions experienced under low shear, which hitherto have been regarded as lying between the ideals of equilibrium flow rheological analysis and industrial reality. The novel technique presented for establishing the time constant of low shear induced structure is straightforward, pragmatic and easily applicable to a wide range of materials. The corelation of this mechanistic timescale, t_{gel}, with the level of viscoelastic structure build under controlled strain applied after high shear, defined by the Weissenberg effect gradient, $\Delta d/\Delta t$, is considered to be a first in the literature. It is predicted that under persistent shear this planar structuration decays into entanglement, and this will be the subject of further investigation by extending the induced hardening effect to greater levels.

ACKNOWLEDGMENTS

This work was supported by the Effnet programme in the Finnish Forest Cluster Ltd.

REFERENCES

1. Isogai, A.; Saito, T.; Fukuzumi, H. *Nanoscale* **2011**, *3*, 71.
2. Herrick, F. W.; Casebier, R. L.; Hamilton, J. K.; Sandberg, K. R. *J. Appl. Polym. Sci.: Appl. Polym. Symp* No. CONF-8205234-Vol. *2*, **1983**; p 37.
3. Spence, K. L.; Venditti, R. A.; Rojas, O. J.; Habibi, Y.; Pawlak, J. J. *Cellulose* **2011**, *18*, 1097.
4. Saito, T.; Nishiyama, Y.; Putaux, J. L.; Vignon, M.; Isogai, A. *Biomacromolecules* **2006**, *7*, 1687.
5. Ahmadzadeh, S.; Nasirpour, A.; Keramat, J.; Hamdami, N.; Behzad, T.; Desobry, S. Nanoporous cellulose nanocomposite foams as high insulated food packaging materials. *Colloids and Surfaces A: Physicochemical and Engineering Aspects* **2015**, *468*, 201.
6. Jorfi, M.; Foster, E. J. *J. Appl. Polym. Sci.* **2015**, *14*, 132.
7. Pinto, R. J.; Carlos, L. D.; Marques, P. A.; Silvestre, A. J.; Freire, C. S. *J. Appl. Polym. Sci.* **2014**, *22*, 131.
8. Ahola, S.; Myllytie, P.; Österberg, M.; Teerinen, T.; Laine, J. *BioResources* **2008**, *3*, 1315.

9. Larsson, K.; Berglund, L. A.; Ankerfors, M.; Lindström, T. *J. Appl. Polym. Sci.* **2008**, *3*, 2460.
10. Iotti, M.; Gregersen, Ø. W.; Moe, S.; Lenes, M. *J. Polym. Environ.* **2011**, *19*, 137.
11. Mohtaschemi, M.; Dimic-Misic, K.; Puisto, A.; Korhonen, M.; Maloney, T.; Paltakari, J.; Alava, M. *Cellulose* **2014**, *21*, 1305.
12. Walls, H. J.; Caines, S. B.; Sanchez, A. M.; Khan, S. A. *J. Rheol.* **2003**, *47*, 847.
13. Coussot, P. In *Rheometry of Pastes, Suspensions, and Granular Materials: Applications in Industry and Environment*; John Wiley and Sons: New Jersey, **2005**.
14. Nechyporchuk, O.; Belgacem, M. N.; Pignon, F. *Carbohydr. Polym.* **2014**, *112*, 432.
15. Grenard, V.; Divoux, T.; Taberlet, N.; Manneville, S. *Soft Matter* **2014**, *10*, 1555.
16. Teece, L. J.; Faers, M. A.; Bartlett, P. *Soft Matter* **2011**, *7*, 1341.
17. Whyte, D.; Walmsley, M.; Liew, A.; Claycomb, R.; Mein, G. *J. Dairy Res.* **2005**, *72*, 115.
18. Ikkala, O.; Ras, R. H.; Houbenov, N.; Ruokolainen, J.; Pääkkö, M.; Laine, J.; Faul, C. F. *Faraday Discuss.* **2009**, *143*, 95.
19. Revol, J. F.; Bradford, H.; Giasson, J.; Marchessault, R. H.; Gray, D. G. *Int. J. Biol. Macromol.* **1992**, *14*, 170.
20. Dong, X. M.; Revol, J. F.; Gray, D. *Cellulose* **1998**, *5*, 19.
21. Lin-Gibson, S.; Kim, H.; Schmidt, G.; Han, C. C.; Hobbie, E. K. *J. Colloid Interface Sci.* **2004**, *274*, 515.
22. Soltero, J. F. A.; Robles-Vásquez, O.; Puig, J. E.; Manero, O. *J Rheol. (N.Y.)* **1995**, *39*, 235.
23. Saito, T.; Uematsu, T.; Kimura, S.; Enomae, T.; Isogai, A. *Soft Matter* **2011**, *7*, 8804.
24. Van de Ven, T. G. M.; Mason, S. G. *Colloid Polym. Sci.* **1977**, *255*, 468.
25. Wang, L.; Tsan, D.; Stoeber, B.; Walus, K. *Adv. Mater. (Weinheim, Ger.)* **2012**, *29*, 3999.
26. Willenbacher, N.; Hanciogullari, H.; Rädle, M. *Tappi, J.* **1999**, *82*, 167.
27. Wollny, K. *Appl. Rheol.* **2011**, *11*, 197.
28. Weissenberg, K. *Math. Phys. Sci.* **1950**, 183.
29. Dimic-Misic, K.; Puisto, A.; Paltakari, J.; Alava, M. J.; Maloney, T. C. *Cellulose* **2013**, *20*, 1853.
30. Dimic-Misic, K.; Puisto, A.; Gane, P. A. C.; Nieminen, K.; Alava, M. J.; Paltakari, J.; Maloney, T. *Cellulose* **2013**, *2*, 2847.
31. Takebe, T.; Hashimoto, T.; Ernst, B.; Navard, P.; Stein, R. S. *J. Chem. Phys.* **1992**, *2*, 1386.
32. Ernst, B.; Navard, P.; Hashimoto, T.; Takebe, T. *Macromolecules* **1990**, *23*, 1370.
33. Vermant, J.; Solomon, M. J. *J. Phys.: Condens. Matter* **2005**, *17*, R187.
34. Eronen, P.; Laine, J.; Ruokolainen, J.; Österberg, M. *J. Colloid Interface Sci.* **2012**, *373*, 84.
35. Saarinen, T.; Haavisto, S.; Sorvari, A.; Salmela, J.; Seppälä, J. *Cellulose* **2013**, *21*, 1261.
36. Horvath, A. E.; Lindström, T. *J. Colloid Interface Sci.* **2007**, *309*, 511.
37. Dimic-Misic, K.; Nieminen, K.; Gane, P. A. C.; Maloney, T. C.; Sixta, H.; Paltakari, J. *Appl. Rheol.* **2014**, *24*, 35616.
38. Fall, A. B.; Lindström, S. B.; Sundman, O.; Ödberg, L.; Wa˚gberg, L. *Langmuir* **2011**, *27*, 11332.
39. Ovarlez, G.; Tocquer, L.; Bertrand, F.; Coussot, P. *Soft Matter* **2013**, *9*, 5540.
40. Chatzimina, M.; Gerogiou, G.; Alexandrou, A. *Appl. Rheology* **2009**, *19*, 34288.
41. Ovarlez, G.; Rodts, S.; Ragouilliaux, A.; Coussot, P.; Goyon, J.; Colin, A. *Phys. Rev. E* **2008**, *78*, 036307.
42. Dukhin, S. S.; Sjöblom, J.; Wasan, D. T.; Sæther, Ø. *Colloids Surf. A: Physicochem. Eng. Aspects* **2001**, *180*, 223.